Inorganic Chemistry
Article

Inorg. Chem. **2010**, *49*, 9599–9608 **9599**
DOI: 10.1021/ic101274q

Mechanism for the Formation of Substituted Manganese(V) Cyanidonitrido Complexes: Crystallographic and Kinetic Study of the Substitution Reactions of *trans*-$[MnN(H_2O)(CN)_4]^{2-}$ with Monodentate Pyridine and Bidentate Pyridine−Carboxylate Ligands

Hendrik J. van der Westhuizen,*,†,§ Reinout Meijboom,*,† Marietjie Schutte,‡ and Andreas Roodt*,‡

†*Department of Chemistry, University of Johannesburg, P.O. Box 524, Auckland Park, 2006, South Africa, and*
‡*Department of Chemistry, University of the Free State, P.O. Box 339, Bloemfontein, 9300, South Africa.*
§*Current address: Sasol Technology, P.O. Box 1, Sasolburg 1947, South Africa*

Received June 26, 2010

Dissolution of $[(CH_3)N]_2Na[MnN(CN)_5]\cdot H_2O$ in water results in the rapid dissociation of the *trans*-CN^- ligand to form *trans*-$[MnN(H_2O)(CN)_4]^{2-}$(aq), which reacts with monodentate pyridine ligands such as 3-methyl and 4-methyl pyridine to form the corresponding mono-substituted complexes, of which the molecular structures obtained from X-ray crystallography, *trans*-$[MnN(3\text{-pic})(CN)_4]^{2-}$ and *trans*-$[MnN(4\text{-pic})(CN)_4]^{2-}$, are reported. $[MnN(H_2O)(CN)_4]^{2-}$(aq) also reacts with bidentate nucleophiles such as pyridine-2-carboxylate (pico) and quinoline-2-carboxylate (quino), yielding the corresponding $[MnN(\eta^2\text{-pico})(CN)_3]^{2-}$ and $[MnN(\eta^2\text{-quino})(CN)_3]^{2-}$ complexes as determined by X-ray crystallography. The formation kinetics of pyridine-2-carboxylate and three different pyridine-2,*x*-dicarboxylate ligands (*x* = 3, 4, 5) are reported, and two consecutive reaction steps are proposed, defined as the formation of the $[MnN(\eta^1\text{-pico})(CN)_4]^{3-}$ and $[MnN(\eta^2\text{-pico})(CN)_3]^{3-}$ complexes, respectively. Only the second steps could be spectrophotometrically observed and kinetically investigated. The first reaction is attributed to the rapid aqua substitution of $[MnN(H_2O)(CN)_4]^{2-}$, thermodynamically unfavored and too fast to observe by conventional rapid third generation stopped-flow techniques. The second, slower reaction is attributed to cyanido substitution, with overall formation rate constants (25 °C; k_1'; $M^{-1}\,s^{-1}$) and corresponding activation parameters ($\Delta H_{k1'}^{\ddagger}$, kJ mol^{-1}, $\Delta S_{k1'}^{\ddagger}$, J K^{-1} mol^{-1}) for the following entering bidentate nucleophiles: pyridine-2-carboxylate: $(1.15 \pm 0.04) \times 10^{-3}$, 102 ± 1, and 48 ± 3; pyridine-2,3-dicarboxylate: $(1.1 \pm 0.1) \times 10^{-3}$, 93 ± 2, and 20 ± 4; pyridine-2,4-dicarboxylate $(8.5 \pm 0.5) \times 10^{-4}$, 123 ± 5, and 115 ± 14; pyridine-2,5-dicarboxylate: $(1.08 \pm 0.04) \times 10^{-3}$, 106 ± 1, and 60 ± 2. A dissociative activation for the cyanido substitution process is proposed.

Introduction

In-depth studies have shown that the aqua ligand in the iso-electronic $[MX(H_2O)(CN)_4]^{n-}$ complexes (M = Mo(IV), W(IV), Tc(V), Re(V); X = O^{2-}, N^{3-}) are all labile toward ligand substitution.[1−5] The rates of substitution depend on the pH of the solution,[6−9] the type of terminal ligand, the central metal atom and to a lesser extent on the type of entering ligand.[10,11]

However, with the exception of crystallographic studies of $(Ph_4P)_2[MnN(CN)_4]\cdot 2H_2O$,[12] $(Ph_4P)_2[MnN(py)(CN)_4]\cdot py\cdot H_2O$,[12] and $[Rh(en)_3][MnN(CN)_5]\cdot H_2O$,[13,14] hardly any studies of manganese tetracyanidonitrido complexes were reported. Results from these structure determinations showed

*To whom correspondence should be addressed. E-mail: roodta@ufs.ac.za.

(1) Leipoldt, J. G.; Basson, S. S.; Roodt, A. In *Advances in Inorganic Chemistry*; Sykes, A. G., Ed; Academic Press: New York, 1993; Vol. *40*, p 297.
(2) Roodt, A.; Abou-Hamdan, A.; Engelbrecht, H. P.; Merbach, A. E. In *Advances in Inorganic Chemistry*; Sykes, A. G., Ed; Academic Press: New York, 2000; Vol. *49*, p 59.
(3) Engelbrecht, H. P.; denDrijver, , L.; Steyl, G.; Roodt, A *C. R. Chim.* **2005**, *8*, 1660.
(4) Engelbrecht, H. P.; Jurisson, S. S.; Cutler, C. S.; den Drijver, L.; Roodt, A. *Synth. React. Inorg. Met.-Org. Nano-Met. Chem.* **2005**, 83.
(5) Roodt, A.; Engelbrecht, H. P.; Botha, J. M.; Otto, S. In *Technetium, Rhenium and Other Metals in Chemistry and Nuclear Medicine*; Nicolini, M., Mazzi, U., Eds.; S G Editorial Publishers: Padova, Italy, 1999; Vol. *5*, p 161.
(6) Roodt, A.; Botha, J. M. *Metal-Based Drugs* **2008**, art. no. 745989.
(7) Leipoldt, J. G.; Basson, S. S.; Roodt, A.; Purcell, W. *Polyhedron Rep. 44* **1992**, *11*, 2277.
(8) Roodt, A; Leipoldt, J. G.; Helm, L.; Merbach, A. E. *Inorg. Chem.* **1994**, *33*, 140.
(9) Abou-Hamdan, A.; Roodt, A; Merbach, A. E. *Inorg. Chem.* **1998**, *37*, 1278.
(10) Roodt, A; Basson, S. S.; Leipoldt, J. G. *Polyhedron* **1994**, *13*, 599.
(11) Purcell, W.; Roodt, A.; Basson, S. S.; Leipoldt, J. G. *Trans. Met. Chem.* **1989**, *14*, 224.
(12) Bendix, J.; Meyer, K.; Weyhermuller, T.; Bill, E.; Metzler-Nolte, N.; Wieghardt, K. *Inorg. Chem.* **1998**, *37*, 1767.
(13) Bendix, I; Deeth, R. J.; Weyhermuller, T.; Bill, E.; Wieghardt, K. *Inorg. Chem.* **2000**, *39*, 930.
(14) van der Westhuizen, H. J.; Roodt, A.; Meijboom, R. *Polyhedron* **2010**, *29*, 470.

Published on Web 09/13/2010

that the complexes have very short terminal nitrido−metal bonds (1.5−1.6 Å). This underlines the significant π-bond character of the metal−nitrogen bond, the nitrido ligand being the strongest π donor known, with the Mn≡N bond in the five-coordinate $[MnN(CN)_4]^{2-}$ anion of 1.507(2) Å the shortest nitrido−metal bond reported to date.[12] More recent work on transition metal nitrido complexes highlighted the special characteristics of this ligand and illustrated reactions to be initiated via attack at the nitride site.[15−24]

With the above in mind, we recently investigated and in a preliminary study reported the behavior of $[MnN(CN)_5]^{2-}$ with respect to the anation reaction with CN^-, N_3^-, and OH^-.[14]

The prime focus of this current study was to investigate the likelihood of complex formation with N-donor monodentate and O,N-donor pyridine-type entering ligands, with the specific aim of determining the bonding modes and substitution sites. We thus describe here the synthesis of tetracyanido(3-methylpyridine)nitridomanganate(V), tetracyanido(4-methylpyridine)-nitridomanganate(V), and tricyanido-nitrido(pyridine-2-carboxylato-κN,κO)manganate(V) as well as tricyanidonitrido-(quinoline-2-carboxylato-κN,κO)manganate(V). The molecular structures of *trans*-$[MnN(3\text{-pic})(CN)_3]^{2-}$, *trans*-$[MnN(4\text{-pic})(CN)_3]^{2-}$, $[MnN(\eta^2\text{-pico})(CN)_3]^{2-}$, and $[MnN(\eta^2\text{-quino})(CN)_3]^{2-}$ are also reported, as well as the formation kinetics of a range of complexes by the reaction of *trans*-$[MnN(H_2O)(CN)_4]^{3-}$ with the pyridine-2-carboxylato ligand and pyridine-2,*x*-dicarboxylate analogues (x = 3, 4, 5). The range of N-donor monodentate and O,N-donor pyridine-type entering ligands was selected to (i) ensure a high solubility of the entering ligand, necessary for the proper investigation of concentration effects and to (ii) include a variation in the Bronsted basicity over more than 2 units of pH. The pK_{a1} values for 3- and 4-methylpyridine are 5.68 and 6.02, respectively, while a value of 5.25 is reported[25,26] for the pK_{a2} of pyridine-2-carboxylic acid. Although not accurately known from the literature, pK_{a2} values of ca. 4.0, 4.5, and 4.4 are estimated for the pyridine-2,*x*-dicarboxylate ligands (x = 3, 4, 5), respectively, on the basis of the corresponding benzene-1,*x*-dicarboxylate analogues (x = 2, 3, 4).[25,26]

Experimental Section

General. All chemicals were obtained from Merck or Sigma-Aldrich and were used as obtained. The UV−vis spectra were recorded on either a Varian Cary 50 or Varian Cary 100 spectrophotometer, and IR spectra were obtained from a Bruker Equinox 55 FT-IR spectrometer and analyzed with Bruker Opus-NT software. NMR spectra were recorded on a Varian Gemini 2000 300 MHz spectrometer (^{1}H: 300 MHz) at ambient temperature.

$(Me_4N)_2Na[MnN(CN)_5]\cdot 2H_2O$ (**1a**) and $(Ph_4Y)_2[MnN(CN)_4]\cdot 2H_2O$ (**1b**) [Y = As, P] were prepared as previously reported[12,14] and are illustrated schematically below.

The intensity data for the X-ray crystallographic studies were collected on a Bruker SMART 1K CCD area detector diffractometer (University of the Witwatersrand) with graphite monochromated Mo Kα radiation (50 kV, 30 mA). The collection method involved ω-scans of 0.3°. Data reduction was carried out using the program SAINT+,[27] and absorption corrections were made using the program SADABS.[27] The structures were solved by the Patterson method, and refinements were done through full-matrix least-squares cycles using the SHELXL-97[28] software package with $\sum(|F_o| - |F_c|)^2$ being minimized. All non-hydrogen atoms were refined anisotropically. Hydrogen atoms were placed in idealized positions and allowed to ride on their parent atom. The program Diamond[29] was used to produce molecular diagrams for the respective complexes, while the densities of the crystals were determined by flotation in benzene/diiodomethane. Crystal data and details of refinement are reported in Table 1.

All reagents and chemicals for the kinetic studies were of analytical grade, and double distilled water was used in all experiments. All the kinetic runs were performed under *pseudo*-first-order conditions with the entering ligand in excess, in a carbonate/hydrogen carbonate buffer medium with the ionic strength adjusted to μ = 1.0 M using KNO_3. No reaction between KNO_3 and *trans*-$[MnN(H_2O)(CN)_4]^{2-}$ could be detected. All pH measurements were recorded on a Hanna pH211 benchtop pH meter equipped with a HI1043B refillable combination glass pH electrode using standard buffer solutions for calibration. The UV/visible absorbance change measurements for the fast kinetic reactions were attempted on a Hi Tech SF61DX2 Stopped Flow System[30] with a thermostatted SHU61DX sample handling unit and an attached Julabu MPV thermostatted water bath (accurate within ±0.05 °C). The UV/vis spectral and absorbance changes for the slow kinetic reactions were measured on Varian Cary 50 Conc and Varian 100 spectrophotometers in 1.000 ± 0.001 cm path length tandem quartz cells. All of the spectrophotometers were equipped with constant temperature cell holders (accurate within 0.1 °C) and Julabu MPV thermostatted water baths (accurate within 0.05 °C) fitted with circulators, and all of the temperatures are reported to ±0.1 °C accuracy. Least-squares analyses were performed on the absorbance vs time data obtained from the kinetics runs (pseudo-first-order conditions and treated as such[6]), spectral changes, and fitting to other functions as defined below, using MicroMath Scientist.[31]

$(Ph_4P)_2[MnN(3\text{-pic})(CN)_4]\cdot 3\text{-pic}$ (2a). $(Ph_4P)_2[MnN(CN)_4]\cdot 2H_2O$ (0.060 g, 0.068 mmol) was dissolved in methanol (~1 cm^3), and 3-methylpyridine (3 cm^3) was added to this solution. The solution was allowed to evaporate at ambient temperature in a fume hood, and pink needles formed. Crystals that were suitable for the X-ray structure determination of this compound were obtained after 2 days. Quantitative yield was obtained. IR (KBr): $\nu_{(Mn\equiv N)}$ = 1040 cm^{-1}, $\nu_{(C\equiv N)}$ = 2114 cm^{-1}. ^{1}H NMR ($CDCl_3$): δ 8.42 (t, 1H); 7.92−7.60 (m, 40H); 7.48 (d, 1H); 7.17 (dd, 1H); 2.33 (s, 3H). UV/vis: λ_{max}, 422 nm; ε, 78 M^{-1} cm^{-1}.

(15) Yi, X.-Y.; Lam, T. C. H.; Sau, Y.-K.; Zhang, Q.-F.; Williams, I. D.; Leung, W. H. *Inorg. Chem.* **2007**, *46*, 7193.
(16) Man, W.-L.; Lam, W. W. Y.; Kwong, H.-K.; Peng, S.-M.; Wong, W.-T.; Lau, T.-C. *Inorg. Chem.* **2010**, *49*, 73.
(17) Izzet, G.; Ishow, E.; Delaire, I; Afonso, C; Tabet, J.-C; Proust., A. *Inorg. Chem.* **2009**, *48*, 11865.
(18) Bendix, I; Birk, T.; Weyhermiiller, T. *Dalton Trans.* **2005**, 2737.
(19) Tran, B. L.; Pink, M.; Gao, X.; Park, H.; Mindiola., D. J. *J. Am. Chem. Soc.* **2010**, *752*, 1458.
(20) Scepaniak, J. J.; Fulton, M. D.; Bontchev, R. P.; Duesler, E. N.; Kirk, M. L.; Smith., J. M. *J. Am. Chem. Soc.* **2008**, *130*, 10515.
(21) Mersmann, K.; Hauser, A.; Lehnert, N.; Tuczek, F. *Inorg. Chem.* **2006**, *45*, 5044.
(22) Martin, A.; Martinez-Espada, N.; Mena, M.; Perez-Redondo, A.; Yelamos, C. *Inorg. Chem.* **2006**, *45*, 6901.
(23) Kwong, H.-K.; Man, W.-L.; Xiang, I; Wong, W.-T.; Lau, T.-C. *Inorg. Chem.* **2009**, *48*, 3080.
(24) Bolzati, C; Cavazza-Ceccato, M.; Agostini, S.; Tisato, F.; Bandoli, G. *Inorg. Chem.* **2008**, *47*, 11972.
(25) Jencks, W. P.; Westheimer, F. H. as reported by Williams, D. A. at http://www.cem.msu.edu/~reusch/Virtual Text/acidity2/htm (accessed Sep 2010).
(26) Brown, H. C. In *Determination of Organic Structures by Physical Methods*; Braude, E. A., Nachod, F. C., Eds.; Academic Press: Nw York, 1955.
(27) *Bruker SAINT+*, version 6.02 (includes XPREP and SADABS); Bruker AXS Inc.: Madison, WI, 1999.
(28) Sheldrick, G. M. *SHELX-97*; University of Gottingen: Gottingen, Germany, 1997.
(29) Brandenburg, K. *Diamond*, Ver. 3.0c; Crystal Impact GbR: Bonn, Germany, 2005.
(30) *KinetAsyst 3.10 Software Package*; Hi-Tech Ltd.: Salisbury, U.K., 2002.
(31) *MicroMath Scientist software for Windows*, Version 2.01; Micromath Inc.: Saint Louis, MO, 1995.

Table 1. Crystal Data and Structure Refinement for $(Ph_4P)_2[MnN(3\text{-pic})(CN)_4]\cdot 3\text{-pic}$, **2a**; $(Ph_4P)_2[MnN(4\text{-pic})(CN)_4]\cdot 0.5(4\text{-pic})\cdot H_2O$, **2b**; $(Ph_4As)_2[MnN(\eta^2\text{-pico})(CN)_4]\cdot 4H_2O$, **3a**; and $(Ph_4As)_2[MnN(\eta^2\text{-quino})(CN)_3]\cdot 3H_2O$, **3b**

	2a	**2b**	**3a**	**3b**
empirical formula	$C_{64}H_{54}N_7P_2Mn$	$C_{61}H_{52.5}N_{6.5}OP_2Mn$	$C_{57}H_{52}N_5O_6As_2Mn$	$C_{61}H_{52}N_5O_5As_2Mn$
fw	1038.02	1009.47	1107.82	1139.86
temp (K)	293	293	273	173
wavelength (Å)	0.71073	0.71073	0.71073	0.71073
cryst syst	triclinic	triclinic	triclinic	triclinic
space group	$P\bar{1}$	$P\bar{1}$	$P\bar{1}$	$P\bar{1}$
unit cell dimensions				
a (Å)	9.606(1)	10.292(2)	13.535(2)	13.401(3)
b (Å)	11.627(1)	13.106(2)	13.790(2)	13.408(3)
c (Å)	25.636(3)	20.557(3)	17.080(2)	17.140(3)
α (deg)	93.878(3)	79.521(3)	87.798(3)	72.09(3)
β (deg)	91.339(3)	87.217(4)	69.375(3)	88.53(3)
γ (deg)	105.962(3)	78.756(4)	61.450(3)	64.62(3)
volume (Å^3)	2743.8(6)	2674.1(7)	2587.9(7)	2627.2(9)
Z	2	2	2	2
D_{exp} (Mg/m^3)	1.25	1.26	1.44	1.41
D_{calc} (Mg/m^3)	1.256	1.254	1.452	1.441
abs coeff (mm^{-1})	0.346	0.354	1.580	1.557
$F(000)$	1084	1054	1136	1168
cryst size (mm^3)	0.23 × 0.10 × 0.05	0.34 × 0.32 × 0.18	0.35 × 0.20 × 0.20	0.36 × 0.28 × 0.16
θ range for data collection (deg)	0.80−26.00	1.01−26.00	1.29−28.50	1.26−26.00
index ranges	$-11 \le h \le 11$ $-14 \le k \le 10$ $-31 \le l \le 30$	$-9 \le h \le 12$ $-16 \le k \le 16$ $-25 \le l \le 24$	$-18 \le h \le 15$ $-18 \le k \le 18$ $-22 \le l \le 22$	$-15 \le h \le 16$ $-16 \le k \le 16$ $-20 \le l \le 21$
reflns collected/unique	16514/10692 /	15957/10424 /	24640/13060/5555	20888/10221/7434
R_{int}	0.0682	0.0606	0.0628	0.0991
completeness to 2θ (deg ; %)	26.00, 99.3	26.00, 99.0	28.50, 99.6	26.00, 98.9
absorption correction	semiempirical from equivalents	semiempirical from equivalents	semiempirical from equivalents	semiempirical from equivalents
max. and min transmission	0.983; 0.959	0.938; 0.877	0.729; 0.691	0.779; 0.599
refinement method	full-matrix least squares on F^2	full-matrix least squares on F^2	full-matrix least squares on F^2	full-matrix least squares on F^2
data/restraints/params	10692/0/668	10424/0/664	13060/0/640	10221/0/667
goodness-of-fit on F^2	0.933	0.925	0.838	1.033
final R indices [$I > 2\sigma(I)$]	R_1 = 0.0601	R_1 = 0.0524	R_1 = 0.0495	R_1 = 0.0642
R indices (all data)	R_1 = 0.1809	R_1 =0.1429	R_1 = 0.1502	R_1 = 0.0919
largest diff. peak and hole	0.231 and −0.263	0.313 and −0.282	1.202 and −0.866	1.782 and −1.084

$(Ph_4P)_2[MnN(4\text{-pic})(CN)_4]\cdot 0.5(4\text{-pic})\cdot H_2O$ (2b). This compound was synthesized analogous to $(Ph_4P)_2[MnN(3\text{-pic})(CN)_4]\cdot 3\text{-pic}$, using 4-methylpyridine instead of 3-methylpyridine. Red crystals were obtained after two days, and they were suitable for the X-ray analysis of this compound. The complex was obtained in quantitative yield. IR (KBr): $\nu_{(Mn\equiv N)}$ = 1043 cm^{-1}, $\nu_{(C\equiv N)}$ = 2127 cm^{-1}. ^{1}H NMR ($CDCl_3$): δ 8.46 (d, 2H); 7.92−7.59 (m, 40H); 7.10 (d, 2H); 2.35 (s, 3H). UV/vis: λ_{max}, 420 nm; ε, 75 M^{-1} cm^{-1}.

Attempted Synthesis of $(Ph_4P)_2[MnN(2\text{-pic})(CN)_4]$ (2c). The attempted synthesis of this compound was analogous to that of $(Ph_4P)_2[MnN(3\text{-pic})(CN)_4]\cdot 3\text{-pic}$ (**2b**), using 2-methylpyridine instead of 3-methylpyridine. Pink crystals were obtained after two days and were suitable for the X-ray analysis of this compound. Yield: 2.8 g (≈70%). Spectral data, IR(KBr): $\nu_{(Mn\equiv N)}$ = 1105 cm^{-1}, $\nu_{(C\equiv N)}$ = 2114 cm^{-1}. ^{1}H NMR ($CDCl_3$): δ7.91−7.57 (m, 40H). UV/vis: λ_{max}, 493 nm; ε, 85 M^{-1} cm^{-1}.

$(Ph_4As)_2[MnN(\eta^2\text{-pico})(CN)_3]\cdot 4H_2O$, (3a). $(Ph_4As)_2[MnN(CN)_4]\cdot 2H_2O$ (0.20 g, 0.20 mmol) was dissolved in ethanol (10 cm^3). Sodium pyridine-2-carboxylate (0.44 g, 3.03 mmol) was dissolved in water (20 cm^3) and the solution added to the $[MnN(CN)_4]^{2-}$ solution. The solution was heated at 70 °C for 8 h. The total volume of the solution was subsequently reduced to *ca.* 5 cm^3 and filtered. Dark red crystals of the title compound suitable for the X-ray structure determination formed after 2 days. Yield: 0.200 g (90%). IR (KBr)/cm^{-1}: $\nu_{(Mn\equiv N)}$. 1033, $\nu_{(C\equiv N)}$ 2124. UV−vis/nm: λ_{max} 350, 520; ε, 2161, 106 M^{-1} cm^{-1}. $\delta_H(CDCl_3)$/ppm: 7.87−7.55 (m, phenyl-H).

$(Ph_4As)_2[MnN(\eta^2\text{-quino})(CN)_3]\cdot 3H_2O$, (3b). $(Ph_4As)_2[MnN(CN)_4]\cdot 2H_2O$ (0.150 g, 0.153 mmol) was dissolved in methanol (10 cm^3). Sodium quinaldinate (0.20 g, 1.02 mmol) was dissolved in water (20 cm^3) and added to the $[MnN(CN)_4]^{2-}$ solution. The resulting solution was heated at 60 °C for 8 h, and the total volume of the solution was reduced to *ca.* 15 cm^3 and filtered. Dark red crystals of the title compound, suitable for X-ray analysis, were obtained after *ca.* 3 days. Yield: 0.157 g (90%). IR(KBr)/cm^{-1}: $\nu_{(Mn\equiv N)}$ 1032, $\nu_{(C\equiv N)}$. 2116. UV/vis: λ_{max}, 370, 525 nm; ε, 2140, 95 M^{-1} cm^{-1}. $\delta_H(CDCl_3)$/ppm: 7.87−7.55 (m, phenyl-H).

In Situ Formation of $[MnN(\eta^2\text{-dipico})(CN)_3]_n$ Complexes (3c−e). These complexes could not be isolated due to high solubilities induced by the ligands but were characterized on the basis of the corresponding observed UV/vis data, compared to those of the corresponding pico and quino complexes described above.

$[MnN(\eta^2\text{-2, 3-dipico})(CN)_3]^{2-}$ (**3c**) UV/vis :

λ_{max}, 356, 521 nm; ε, 1750, 97 M^{-1}cm^{-1}

$[MnN(\eta^2\text{-2, 4-dipico})(CN)_3]^{2-}$ (**3d**) UV/vis :

λ_{max}, 375, 524 nm; ε, 2020, 101 M^{-1} cm^{-1}

$[MnN(\eta^2\text{-2, 5-dipico})(CN)_3]^{2-}$ (**3e**) UV/vis :

λ_{max}, 383, 527 nm; ε, 1630, 94 M^{-1} cm^{-1}

Reaction Mechanism and Kinetic Data Analysis. The overall reaction, describing the substitution process of the aqua and a

Scheme 1. The Protonation and Mono/Bidentate Substitution (N−O = Picolinate Type Ligands) Reaction Scheme for the $[MnN(H_2O)(CN)_4]^{2-}$ Complex

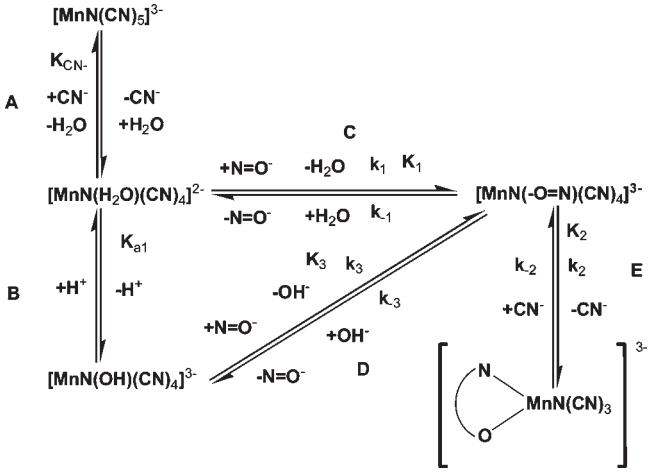

cyanido ligand in $[MnN(H_2O)(CN)_4]^{2-}$ by entering bidentate ligands, is given in Scheme 1.[10] In the case of methyl pyridine type monodentate ligands, only steps C and D are observed, and step E does not take place; i.e., the substitution of an equatorial cyanide ligand is not observed, even in a *large* excess of methyl pyridine.

Complete derivation of the thermodynamic and kinetic equations given below are available as Supporting Information.

The overall stability constant (denoted by K') for the complete reaction between the $[MnN(H_2O)(CN)_4]^{2-}$ complex and the pyridine-2-carboxylate type ligands (indicated by N=O$^-$), as described in Scheme 1, is given by eq 1,[32] which is derived from Beer's law, mass balance, and the definition of K' for the overall reaction. In eq 1, A_M and A_{ML} represent the absorbances of the $[MnN(H_2O)(CN)_4]^{2-}$ and $[MnN(\eta^2\text{-pico})(CN)]^{2-}$ complexes, A_{obs} the observed absorbance, and [N=O$^-$] the concentration of the pyridine-2-carboxylate-type ligands.

$$A_{obs} = (A_M + A_{ML}K'[N{=}O^-])/(1 + K'[N{=}O^-]) \quad (1)$$

The concentration dependence of the pseudo-first-order rate constant (k_{obs}) for the second, slower ring-closing step by bidentate chelators such as pyridine-2-carboxylate-type ligands is described by eq 2,[46] assuming (i) a small equilibrium constant and a rapid first step for the formation of the hapto-1 complex and (ii) monitoring of the kinetics at conditions where [N=O$^-$] ≫ [Mn] and where the $[MnN(H_2O)(CN)_4]^{2-}$ species is the only Mn(V) complex in solution ($K_{al} \ll [H^+]$).

$$k_{obs} = k_1'[N{=}O^-] + k_{-1}' \quad (2)$$

However, in more basic solutions, where the hydoxo species' concentration becomes appreciably higher, the more complete rate equation for the pseudo-first-order rate constant is given by eq 3,[10] thus also incorporating the acid dissociation constant, K_{a1}, of the $[MnN(H_2O)(CN)_4]^{2-}$ species. The second-order rate constants k'_1 and k'_3 then represent the combined rate constants for the aqua and the hydroxo species undergoing bidentate chelation, respectively.

$$k_{obs} = \{k_1' + k_3'(K_{a1}/[H^+])\}[N{=}O^-]/(1 + K_{a1}/[H^+]) + k_{-1}' \quad (3)$$

Results and Discussion

Synthesis. It is somewhat surprising that the tetracyanidonitrido complexes of Mn(V)[12,13] have received so little attention to date, whereas the corresponding analogues of Tc(V), Re(V), and Os(VI) are known and have been widely studied. Specifically, *trans*-$[TcN(OH_2)(CN)_4]^{2-}$,[33] *trans*-$[ReN(OH_2)(CN)_4]^{2-}$,[34] *trans*-$[ReN(CN)_5]^{3-}$,[35] *trans*-$[ReN(N_3)(CN)_4]^{3-}$,[36] and *trans*-$[OsN(OH)(CN)_4]^{2-}$ [37] have been synthesized, and the PPh_4^+ or $AsPh_4^+$ salts of these anions have been crystallographically characterized.

Scheme 2. Synthesis of Compounds **2a**, **2b**, **3a**, and **3b**

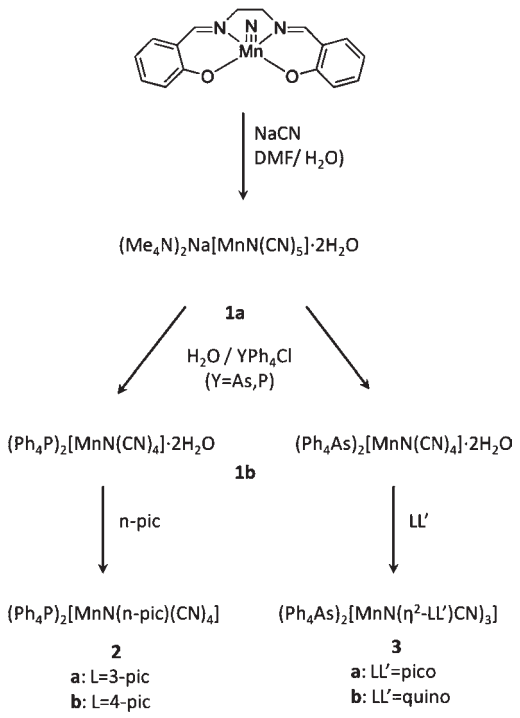

Fairly simple synthetic routes are known for the synthesis of the complexes *trans*-$[MN(CN)_4]^{n-}$ (M = Tc, Re, Os). It seems, however, that only a limited number of synthetic routes are available for the synthesis of the tetracyanidonitrido complexes of manganese(V).[38] We followed the route reported a decade ago, which synthesizes the tetracyanidonitrido complexes of Mn(V) by ligand substitution of the salen ligand from $[Mn^VN(salen)]$ by CN$^-$ in aqueous solutions of NaCN[12] (Scheme 2).

Good yields were obtained for the products **2a**, **2b**, **3a**, and **3b**, displaying typical spectroscopic data when compared to analogous periodic complexes. Confirmation of the molecular structures, however, unequivocally comes from the X-ray analysis as described below.

(32) Roodt, A.; Leipoldt, J. G.; Deutsch, E. A.; Sullivan, J. C. *Inorg. Chem.* **1992**, *31*, 1080.

(33) Baldas, J.; Boas, J. F.; Colmanet, S. F.; Mackay, M. F. *Inorg. Chim. Acta* **1990**, *170*, 233.

(34) Purcell, W.; Potgieter, I. M.; Damoense, L. J.; Leipoldt, J. G. *Trans. Met. Chem.* **1992**, *17*, 387.

(35) Purcell, W.; Potgieter, I. M.; Damoense, L. J.; Leipoldt, J. G. *Trans. Met. Chem.* **1991**, *16*, 473.

(36) Purcell, W.; Damoense, L. J.; Leipoldt, J. G. *Inorg. Chim. Acta* **1992**, *195*, 217.

(37) Van der Westhuizen, H. J.; Basson, S. S.; Purcell, W. *Trans. Met. Chem.* **1994**, *19*, 582.

(38) (a) Arshankov, S. I.; Poznjak, A. L. *Z. Anorg. Allg. Chem.* **1981**, *481*, 201. (b) Buchler, J. W.; Dreher, C; Lay, K.-L. *Z. Naturforsch., B.* **1982**, *37B*, 1155. (c) Hill, C. L.; Hollander, F. J. *J. Am. Chem. Soc.* **1982**, *104*, 7318. (d) Buchler, J. W.; Dreher, C; Lay, K.-L.; Lee, Y. J. A.; Scheidt, W. R. *Inorg. Chem.* **1983**, *22*, 888. (e) Du Bois, J.; Tomooka, C. S.; Hong, J.; Carreira, E. M.; Day, M. W. *Angew. Chem., Int. Ed. Engl.* **1997**, *36*, 1645. (f) Niemann, A.; Bossek, U.; Haselhorst, G.; Wieghardt, K.; Nuber, B. *Inorg. Chem.* **1996**, *35*, 906. (g) Du Bois, J.; Tomooka, C. S.; Hong, J.; Carreira, E. M. *Acc. Chem. Res.* **1997**, *30*, 364.

Attempted synthesis of $(Ph_4P)_2[MnN(2\text{-pic})(CN)_4]\cdot 2H_2O$ (**2c**) did not yield a product containing 2-methylpyridine (2-pic), as confirmed by proton NMR. It was then anticipated that the illusive *trans*-$[MnN(H_2O)(CN)_4]^{2-}$ might have been obtained; however, subsequent single crystal XRD revealed that the five-coordinate complex, $[MnN(CN)_4]^{2-}$, was yet again isolated. The reader is therefore referred to the original structure[12] for further details regarding the spectroscopy and single-crystal X-ray data.

A possible reason for the isolation of the $(Ph_4P)_2[MnN(CN)_4]\cdot 2H_2O$ complex instead of the $(Ph_4P)_2[MnN(2\text{-pic})(CN)_4]$ complex is attributed to the very low stability constant (K_1) of the 2-pic complex, or alternatively, a lower crystallization energy of $(Ph_4P)_2[MnN(CN)_4]$ compared to $(Ph_4P)_2[MnN(2\text{-pic})(CN)_4]$ or the *trans*-$[MnN(H_2O)(CN)_4]^{2-}$. Regardless, isolation of the five-coordinate complex again points to the weak $Mn-OH_2$ interaction in the aqua species, assumed to be present in an aqueous medium, and the extremely rapid kinetics observed underlines the lability for ligation trans to the nitrido ligand, see the further discussion below.

The UV−vis spectrum obtained from the reaction between $[MnN(H_2O)(CN)_4]^{2-}$ and pyridine-2-carboxylate ($pico^-$) anions showed a strong absorbance maximum at 350 nm, whereas the pyridine-2,*x*-dicarboxylate (2,*x*-$dipico^{2-}$) anions showed maxima at $\lambda = 356$ nm for 2,3-$dipico^{2-}$ and $\lambda = 375$ and 383 nm for 2,4-$dipico^{2-}$ and 2,5 $dipico^{2-}$, respectively. The kinetics of the reaction between $[MnN(H_2O)(CN)_4]^{2-}$ and 2-quinoline-carboxylate (quino) could not be studied due to low product solubility and smaller absorbance changes, thus yielding less accurate kinetic results.

It is clear that all four structures, **2a**, **2b**, **3a**, and **3b**, consist of well separated $(Ph_4P)^+$ or $(Ph_4As)^+$ cations and well-defined $[MnN(L)(CN)_4]^{2-}$ (L = 3-pic; 4-pic) or $[MnN(\eta^2\text{-}LL')(CN)_3]^{2-}$ (LL′ = η^2-pico; η^2-quino) complex anions and solvate/hydrate molecules. The bond distances and angles within the two $(Ph_4P)^+$ cations are normal and in good agreement with those found in the previous reported structure determinations containing these cations.[12,39−41]

Molecular Structures of Complexes with Monodentate Ligands 3- and 4-Methylpyridine. Molecular diagrams showing the numbering schemes of the complex anions of $(Ph_4P)_2[MnN(3\text{-pic})(CN)_4]\cdot(3\text{-pic})$, **2a**, and $(Ph_4P)_2[MnN(4\text{-pic})(CN)_4]\cdot 0.5(4\text{-pic})\cdot H_2O$, **2b**, are presented in Figure 1. Both compounds crystallize in the triclinic space group, $P\bar{1}$, with $Z = 2$.

The structure of $(Ph_4P)_2[MnN(3\text{-pic})(CN)_4]\cdot(3\text{-pic})$, **2a**, contains 3-methylpyridine solvate molecules, but not situated in close proximity to the complex anion molecule, and thus no strong hydrogen bonding interactions between these moieties are observed. Moreover, no water molecules of crystallization were detected. The hydrate present in the crystals of $(Ph_4P)_2[MnN(py)(CN)_4]\cdot py\cdot H_2O$[12] exhibited weak hydrogen-bonding contacts to one of the nitrogen atoms of a cyanido group of the complex anion and the nitrogen atom of the pyridine molecule of crystallization,

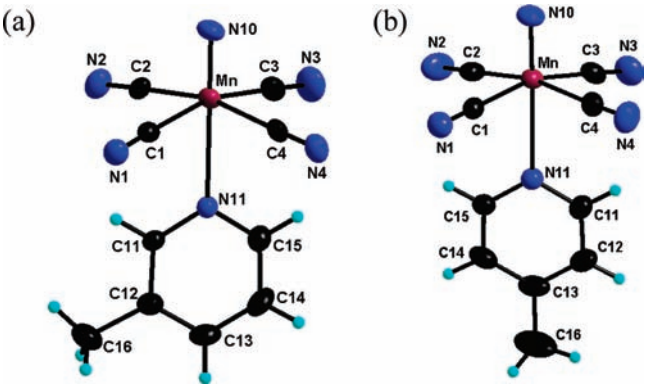

Figure 1. Molecular diagrams showing the numbering scheme and displacement ellipsoids (30% probability) of the (a) *trans*-$[MnN(3\text{-pic})(CN)_4]^{2-}$ and (b) *trans*-$[MnN(4\text{-pic})(CN)_4]^{2-}$ complex anions. The cations and solvate molecules are omitted for clarity.

but the trend was not observed in the crystal structure of $(Ph_4P)_2[MnN(3\text{-pic})(CN)_4]\cdot(3\text{-pic})$.

In contrast to the above, the structure of $(Ph_4P)_2[MnN(4\text{-pic})(CN)_4]\cdot 0.5(4\text{-pic})\cdot H_2O$ (**2b**) contains both 4-methylpyridine and water solvate molecules. The hydrate forms weak intermolecular hydrogen-bonding contacts [O(1W)···N(2) = 2.959(5) Å] to one of the cyanido ligands of the $[MnN(4\text{-pic})(CN)_4]^{2-}$ complex anion, but no interaction between itself and the 4-methyl pyridine molecule was detected. It is interesting that the nitrido ligand does not exhibit any interactions with the solvate molecules, which might suggest that the former has a low basicity compared to the nitrogen atoms of the *cis*-bonded cyanido ligands.

The complex anions *trans*-$[MnN(3\text{-pic})(CN)_4]^{2-}$ and *trans*-$[MnN(4\text{-pic})(CN)_4]^{2-}$ are very similar, also in terms of interatomic bond distances and angles, see Table 2. The Mn≡N bonds are short at 1.51−1.52 Å with the Mn−CN bonds around 1.99 Å and approximate linear Mn−C−N entities. The Mn−N (methyl pyridine) bonds are very long at ca. 2.43 Å, indicative of weak coordination by the 3-pic and 4-pic trans to the nitrido ligand. The bonds within the 3-pic and 4-pic ligands are similar and normal compared to other data.

The interatomic bond angles are also normal, with the angles "above" the cyanido−carbon plane, between the nitrido and the cyanide ligands, around 98° and those below the plane, the approximate supplements, at 82−83°. The N≡Mn−N (nitrido-methyl pyridine) moieties are approximately linear, while the in-plane NC−Mn−CN angles approximate 90°. However, the NC−Mn−CN angles deviate significantly from linearity and are around 165°.

Molecular Structures of Complexes with Bidentate Ligands Pyridine-2-Carboxylate and Quinoline-2-Carboxylate (pico and quino). Molecular diagrams showing the numbering schemes of the anions of compound **3a** ($(Ph_4As)_2[MnN(\eta^2\text{-pico})(CN)_3]\cdot 4H_2O$) and **3b** ($(Pl_4As)_2[MnN(\eta^2\text{-quino})(CN)_3]\cdot 4H_2O$) are presented in Figure 2, with selected bond lengths, angles, and torsion angles reported in Table 3. Both compounds crystallize in the triclinic space group, $P\bar{1}$, with $Z = 2$. Comparative bond distances and angles for selected related compounds are given in Table 4.[42,43]

(39) Purcell, W.; Potgieter, I. M.; Damoense, L. J.; Leipoldt, J. G. *Trans. Met. Chem.* **1991**, *16*, 473.
(40) Purcell, W.; Roodt, A.; Basson, S. S.; Leipoldt, J. G. *Trans. Met. Chem.* **1989**, *14*, 5.
(41) Leipoldt, J. G.; Basson, S. S.; Roodt, A.; Potgieter, I. M. *Trans. Met. Chem.* **1986**, *77*, 323.
(42) Van der Westhuizen, H. J.; Roodt, A; Meijboom, R. Unpublished results.
(43) Mtshali, T. N.; Purcell, W. P.; Visser, H. G.; Basson, S. S. *Polyhedron* **2006**, *25*, 2415.

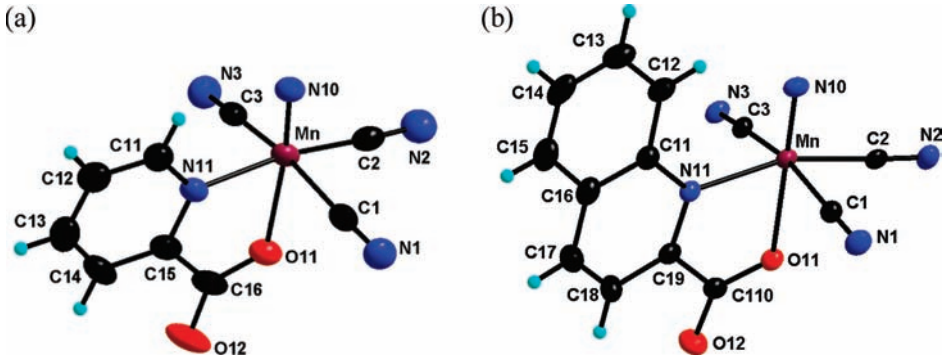

Figure 2. Molecular diagrams showing the numbering scheme and displacement ellipsoids (30% probability) of the (a) $[MnN(\eta^2\text{-pico})(CN)_3]^{2-}$ and (b) $[MnN(\eta^2\text{-quino})(CN)_3]^{2-}$ anion. The cations and solvate molecules are omitted for clarity.

Table 2. Selected representative bond distances (Å) and angles (°) in the complexes *trans*-$[MnN(3\text{-pic})(CN)_4]^{2-}$ **2a**, and *trans*-$[MnN(4\text{-pic})(CN)_4]^{2-}$ **2b**

bond	**2a**	**2b**
	Bond Distances (Å)	
Mn−N(10)	1.523(4)	1.514(3)
Mn−C(1)	1.996(5)	1.997(4)
Mn−C(3)	1.992(5)	1.990(4)
Mn−N(11)	2.431(4)	2.429(3)
C(1)−N(1)	1.150(5)	1.149(4)
C(3)−N(3)	1.151(5)	1.144(4)
C(12)−C(16)	1.514(7)	1.521(5)[a]
N(11)−C(11)	1.348(5)	1.318(4)
N(11)−C(15)	1.318(5)	1.334(4)
	Bond Angles (deg)	
N(10)−Mn−C(1)	97.84(19)	97.99(16)
N(10)−Mn−N(11)	179.44(18)	177.53(14)
C(1)−Mn−N(11)	81.66(15)	82.50(12)
C(3)−Mn−C(1)	164.50(19)	163.69(14)
C(2)−Mn−C(1)	89.75(18)	90.79(15)
N(1)−C(1)−Mn	176.2(4)	178.6(3)
C(15)−N(11)−Mn	121.7(3)	121.5(2)

[a] C(13)−C(16).

Table 3. Selected Representative Bond Distances (Å) and Angles (deg) in the Complexes $[MnN(\eta^2\text{-pico})(CN)_3]^{2-}$, **3a**, and $[MnN(\eta^2\text{-quino})(CN)_3]^{2-}$, **3b**

	3a (pico)	**3b** (quino)
	Bond Distances (Å)	
Mn−N(10)	1.538(3)	1.523(5)
Mn−C(1)	1.998(5)	2.003(5)
Mn−C(2)	1.931(5)	1.984(5)
Mn−C(3)	1.999(5)	1.999(5)
Mn−N(11)	2.045(3)	2.110(4)
Mn−O(11)	2.214(3)	2.168(4)
N(11)−C(11)	1.345(5)	1.404(6)
C(1)−N(1)	1.154(5)	1.157(7)
C(2)−N(2)	1.150(5)	1.136(7)
C(3)−N(3)	1.142(5)	1.161(6)
N(11)−C(15)	1.354(5)	1.331(7)[a]
	Bond Angles (deg)	
N(10)−Mn−C(1)	97.91(18)	96.2(2)
N(10)−Mn−C(3)	98.84(17)	97.3(2)
N(10)−Mn−O(11)	171.93(16)	178.88(19)
N(10)−Mn−C(2)	97.27(18)	94.9(2)
N(10)−Mn−N(11)	95.85(17)	103.9(2)
C(2)−Mn−C(1)	85.99(17)	87.8(2)
C(2)−Mn−C(3)	86.74(18)	88.8(2)
C(1)−Mn−C(3)	162.45(18)	166.3(2)
N(11)−Mn−O(11)	76.12(13)	76.37(15)
C(1)−Mn−N(11)	93.96(15)	88.78(18)
C(3)−Mn−N(11)	89.51(15)	90.17(18)
C(2)−Mn−N(11)	166.76(17)	161.2(2)
C(1)−Mn−O(11)	82.15(15)	84.88(18)
C(3)−Mn−O(11)	81.99(14)	81.58(18)
C(2)−Mn−O(11)	90.78(16)	84.87(18)
N(1)−C(1)−Mn	175.9(4)	178.7(4)
C(11)−N(11)−Mn	124.2(3)	128.0(3)
C(15)−N(11)−Mn	117.5(3)	115.1(3)[b]

[a] N(11)−C(19). [b] C(19)−N(11)−Mn.

Both molecular structures of $(Ph_4As)_2[MnN(\eta^2\text{-pico})(CN)_3]\cdot 4H_2O$ and $(Ph_4As)_2[MnN(\eta^2\text{-quino})(CN)_3]\cdot 4H_2O$ consist of discrete $(Ph_4As)^+$ cations and Mn(IV) complex anions. The bond distances and angles within the $(Ph_4As)^+$ cations were normal and in good agreement with those found in other crystal structures.[34,37,41]

The Mn(V) atom is octahedrally coordinated to a nitrido ligand, three cyanido ligands, and the nitrogen atom of the aromatic ring as well as one of the oxygen atoms of the carboxylate group of the picolinate/quinolinate ligand in the $[MnN(\eta^2\text{-pico})(CN)_3]^{2-}$ and the $[MnN(\eta^2\text{-quino})(CN)_3]$ anions. The nitrogen atom of the picolinate/quinolinate ligand is in the equatorial plane trans to a cyanido ligand, and the oxygen atom is axial approximately *trans* to the nitrido ligand. The very short Mn≡N bond distance of ca. 1.53 Å suggests strong pπ−dπ ligand-to-metal interaction. The Mn−C bond of the cyanido ligand which is coordinated ca. *trans* to the nitrogen atom of the picolinate ligand in $MnN(\eta^2\text{-pico})(CN)_3]^{2-}$ is significantly longer than the other two Mn−CN bonds, while the corresponding bond in the $[MnN(\eta^2\text{-quino})(CN)_3]^{2-}$ anion is comparable to the other two Mn−C bond distances of the other two cyanido ligands.

The Mn−C−N moieties are nearly linear, with an average bond angle of 176.6(4)°. The Mn−N(11) and the Mn−O(11) bond distances are 2.045(3) Å and 2.214(3) Å, for the picolinate ligand, and reversed at 2.110(4) Å and 2.168(4) Å, respectively, for the quinolinate ligand. The longer than expected Mn−O(11) bond distance is an indication of the large *trans*- influence of the nitrido ligand.

The interatomic bond angles are also normal, with the angles "above" the cyanido−carbon plane, between the nitrido and the cyanide ligands around 98−98°, and those below the plane, the approximate supplements, at 86−89°. The N≡Mn−O (carboxylato) angle deviates

Table 4. Comparison of Structural Parameters (Å, deg) in Isostructural Related $[MX(\eta^2\text{-pico/quino})(CN)_3]^{n-}$ (M = Mn, Re, X = N; M = Mo, W; X = O) Anions

anion	M≡N or M=O (Å)	M−O[a] (Å)	D[b] (Å)	bite angle (deg)	M−N[c] (Å)	M−C[d] (Å)	N(10)−M−O(11) angle (deg)	$\nu_{(MX)}$ (cm^{-1})
3a[f]	1.538(3)	2.214(3)	0.259(2)	76.1(1)	2.045(3)	1.931(5)	171.9(2)	1033
3b[f]	1.523(5)	2.168(4)	0.286(3)	76.4(2)	2.110(4)	1.984(5)	178.9(2)	1032
ReN(pico)[g]	1.655(3)	2.067(5)	0.298(1)	72.4(1)	2.169(3)	2.067(5)	166.5(1)	1061
MoO(pico)[h]	1.681(3)	2.216(4)	0.309(2)	72.1(1)	2.216(4)	2.125(6)	161.9(2)	944
WO(pico)[i]	1.676(9)	2.171(8)	0.331(2)	72.5(4)	2.188(13)	2.042(18)	164.7(5)	944

[a] *trans* to M=N or M=O bonds. [b] Displacement of the central metal atom from the plane formed by the three carbon atoms of the cyanido ligands and the nitrogen atom of the bidentate ligand. [c] M−N bond of the bidentate ligand *trans* to the cyanido ligand in equatorial plane. [d] M−C bond of the cyanido ligand *trans* to the nitrogen atom of the bidentate ligand in the equatorial plane. [e] *trans*-N≡M−O bond. [f] This work. [g] Ref 43. [h] Ref 42. [i] Ref 41.

from linearity at 171.93(16)°, suggesting an in-plane rotation (parallel to the planar pico ligand aromatic structure plane). However, for the $[MnN(\eta^2\text{-quino})(CN)_3]^{2-}$ complex anion, the N≡Mn−O (carboxylato) angle at 178.88(19)° indicates a normal close to linearity for the trans coordination mode. The in-plane NC−Mn−CN angles are approximately 90°, while the NC−Mn−CN angles deviate significantly from linearity and are around 162−166°. The pico and quino N−Mn−O bite angles, for both the complexes, are small and almost identical at *ca.* 76°.

The metal center in the $[MnN(\eta^2\text{-pico/quino})(CN)_3]^{2-}$ anions is displaced by 0.259(2) and 0.286(3) Å from the plane formed by the carbon atoms of the three cyanido ligands and the nitrogen atom of the picolinate/quinolinate ligand toward the nitrido ligand, for the picolinate and quinolinate ligand, respectively, and compare well with similar complexes, see Table 4. This distortion is attributed to a strong π-bonded ligand such as an oxide or nitrido ligand bonded in an axial position of an octahedral transition metal complex. The displacement of the manganese(V) metal atom toward the nitrido ligand corresponds with the similar displacement (0.331 Å) found for the $[WO(pico)(CN)_3]^{2-}$ anion.[41]

Upon reaction of the $[MnN(H_2O)(CN)_4]^{2-}$ complex with monodentate entering ligands, the monosubstituted complexes are formed, as confirmed by the crystal structure determinations of *trans*-$[MnN(3\text{-pic})(CN)_4]^{2-}$ (**2a**) and *trans*-$[MnN(4\text{-pic})(CN)_4]^{2-}$ (**2b**) as reported above. Similarly, the crystal structure determinations of both the $(Ph_4As)_2[MnN(\eta^2\text{-pico})(CN)_3]\cdot 4H_2O$ (**3a**) and $(Ph_4As)_2[MnN(\eta^2\text{-quino})(CN)_3]\cdot 3H_2O$ (**3b**) complexes showed that, in both final products from the reactions of $[MnN(H_2O)(CN)_4]^{2-}$ with pico$^-$ and quino$^-$ ligands, respectively, the pyridine carboxylate-type ligands coordinate to the manganese(V) metal center with the oxygen atom of the carboxylate group *trans* to the nitrido ligand and that the pyridine nitrogen atom substituted an equatorial cyanido ligand.

Equilibrium Studies. The results of the crystal structure determination of the $[MnN(\eta^2\text{-pico})(CN)_3]^{2-}$ complex indicate that the first step in Scheme 1 (reaction C) is the substitution of an *aqua* ligand by the oxygen atom of the carboxylate group (k_1 path) with the formation of the $[MnN(\eta^1\text{-pico})(CN)_4]^{3-}$ complex. Subsequent substitution of one equatorial cyanido ligand by the nitrogen atom of the pyridine moiety (k_2 path, reaction E) and the resultant formation of the $[MnN(\eta^2\text{-pico})(CN)_4]^{2-}$ complex completes the chelate ring formation. This is analogous to the reaction between $[WO(H_2O)(CN)_4]^{2-}$ and pico$^-$, where a value of the equilibrium constant for the formation of the hapto-1 complex, $K_1 = 1.1(2)\ M^{-1}$,[1,10,44] was obtained. For the *aqua* substitution by the carboxylate moiety of pico$^-$ onto the manganese(V) complex in the current study, this equilibrium is also assumed to be small and very rapid ($k_{obs} > 1000\ s^{-1}$ at 0.1 M [entering ligand]; indicating a second-order rate constant of $> 10^4\ M^{-1}\ s^{-1}$) since no reaction could be detected even by third-generation stopped-flow techniques. The equilibrium constant, K_1, reported for the reaction between $[MoO(H_2O)(CN)_4]^{2-}$ and phen [$K_1 = 5.6(3) \times 10^2\ M^{-1}$][45] was incorrectly assigned to the aqua substitution only but was later corrected as the *overall* equilibrium constant [representing both steps 1 and 2 in Scheme 1], since only one reaction was observed and it was initially thought that *aqua* substitution is the rate-determining step of the two-step process.

The thermodynamic stability constant (K', Table 5) for the *overall* reaction between the $[MnN(H_2O)(CN)_4]^{2-}$ complex and the pyridine-2-carboxylate-type ligands was determined by means of UV−vis spectrophotometry at 350 nm from a least-squares fit of the absorbance vs concentration data shown in Figure 3 to eq 1.[46]

Kinetics. Analysis of the absorbance vs time data for the individual kinetic traces in this study clearly indicated that only one overall reaction is observed for all studied ligands. The temperature and concentration dependence of the *pseudo*-first-order rate constant (k_{obs}) for the second, slow, reaction at λ 350 nm for the pyridine-2-carboxylate ligand is shown in Figure 4. The k_{obs} vs [pico$^-$] data in Figure 4 were fitted to eq 2,[10] and the values of k_1' ($k_1' = k_2K_1$) and k'_{-1} are reported in Table 5 for a temperature range for the different bidentate ligands studied. The term k_{-1}' represents the contribution of the reverse reaction or the recoordination of the cyanide anion. However, the influence of this rate constant (k_{-1}') could not be determined due the fact that only a very small excess of added cyanide anions severely retarded the rate of the reaction between $[MnN(H_2O)(CN)_4]^{2-}$ and pyridine-2(*x*-di)carboxylate (di)anions. The kinetics are therefore complicated due to the fact that the addition of excess free CN$^-$ leads to the formation of the $[MnN(CN)_5]^{3-}$; the reverse reaction in the initial equilibrium for the formation of the $[MnN(H_2O)(CN)_4]^{2-}$ complex from $[MnN(CN)_5]^{3-}$ (see reaction A, Scheme 1).

The *pseudo*-first-order rate constant for the second reaction is pH dependent (see Figure 5 and Supporting Information). The acid dissociation constant for the

(44) Roodt, A; Leipoldt, J. G.; Helm, L.; Merbach, A. E. *Inorg. Chem.* **1992**, *31*, 2864.

(45) Leipoldt, J. G.; Basson, S. S.; Potgieter, I. M.; Roodt, A. *Inorg. Chem.* **1987**, *26*, 57.

(46) Roodt, A; Leipoldt, J. G.; Deutsch, E. A.; Sullivan, J. C. *Inorg. Chem.* **1992**, *31*, 1080.

Table 5. Kinetic Data for the Reactions between Pyridine-2-Carboxylate (pico) and Pyridine-2,(*x*)-dicarboxylate (*x* = 3, 4, 5; dipico) and $[MnN(H_2O)(CN)_4]^{2-}$

constant	pico$^-$	2,3-dipico^{2-}	2,4-dipico^{2-}	2,5-dipico^{2-}
	25.6 °C	24.9 °C	25.2 °C	25.4 °C
K'^a	33(4)	6.4(6)	30(4)	43(4)
k'_1 (M^{-1} s^{-1})^b	1.15(4) × 10^3	1.11(1) × 10^{-3}	8.5(5) × 10^{-4}	1.08(4) × 10^{-3}
k'_{-1} (s^{-1})^c	3.1(1) × 10^{-5}	7.2(2) × 10^{-5}	3.2(1) × 10^5	5.5(1) × 10^{-5}
K'_1 (M^{-1})^d	37(1)	15(1)	27(2)	20(1)
pK_{a1}^{e}	13.6(6)	13.3(2)		
	35.7 °C	36.6 °C	35.1 °C	35.4 °C
k'_1 (M^{-1} s^{-1})^b	5.0(1) × 10^{-3}	6.1(2) × 10^{-3} ^{f}	3.1(2) × 10^{-3}	5.6(1) × 10^{-3}
k'_{-1} (s^{-1})^c	1.16(l) x 10^{-4}	4.2(1) × 10^{-4} ^{f}	1.2(1) × 10^{-4}	1.94(4) 10^{-4}
K'_1 (M^{-1})^d	43(2)	15(l)^f	26(2)	29(1)
	45.6 °C	45.5 °C	45.3 °C	45.4 °C
k'_1 (M^{-1} s^{-1})^b	0.0199(5)	0.023(l)^g	0.017(1)	0.0201(6)
k'_{-1} (s^{-1})^c	4.0(1) × 10^{-4}	1.39(3) × 10^{-3} ^{g}	4.0(3) × 10^{-3}	6.9(2) × 10^{-4}
	54.6 °C	55.0 °C		55.0 °C
k'_1 ($M^{-1}s^{-1}$)	0.063(2)^i	0.071(2)^{j,h}		0.065(2)^k
k'_{-1} (s^{-1})	1.2(1) × 10^{-3} ^{i}	4.9(2) × 10^{-3} ^{j,h}		2.5(1) × 10^{-3} ^{k}
	74.6 °C			
k'_1 ($M^{-1}s^{-1}$)	0.60(2)^i			
k'_{-1} (s^{-1})	1.1(1) × 10^{-2} ^{i}			
$\Delta H_{k'1}^{\ddagger}$ (kJ mol^{-1})^l	102(1)	93(2)	123(5)	106(1)
$\Delta S_{k'1}^{\ddagger}$ (J K^{-1} mol^{-1})^l	48(3)	20(4)	115(14)	60(2)
$\Delta H_{k'1}^{\ddagger}$ (kJ mol^{-1})^m	104(3)	103(3)	*n*	104(3)
$\Delta S_{k'1}^{\ddagger}$ (J K^{-1} mol^{-1})^m	55(7)	52(10)	*n*	55(10)

^{a} A_{obs} vs [N=O$^-$] data fitted to eq 1 and Supporting Information. ^{b} Slopes from lines fitted to eq 2 and Supporting Information. ^{c} The *y* intercepts of lines fitted to eq 2; Figure 4 and Supporting Information. ^{d} $K_1' = k_1'/k_{-1}'$. ^{e} Data fitted to eq 2; Figure 5 and Supporting Information. ^{f} 40 °C. ^{g} 50 °C. ^{h} 60 °C. ^{i} Calculated from eq 2; assume $K_1' = 43$ M^{-1}. ^{j} Calculated from eq 2; assume $K_1' = 15$ M^{-1}. ^{k} Calculated from eq 2; assume $K_1' = 25$ M^{-1}. ^{l} Exponential form of Earing equation; see also Figure 6. ^{m} Global fit utilizing combined model incorporating exponential form of Eyring equation and individual k_{obsd} values (Supporting Information) in eq 2. ^{n} Not enough data points for reliable global fit.

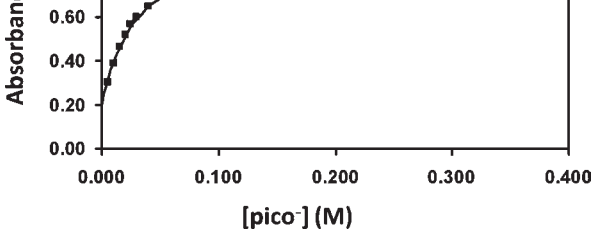

Figure 3. Absorbance vs [pico$^-$] at 25.6 °C, $[Mn]_T = 5.26 \times 10^{-4}$ M, μ = 1.0 M (KNO_3), pH = 10.0, λ = 350.0 nm.

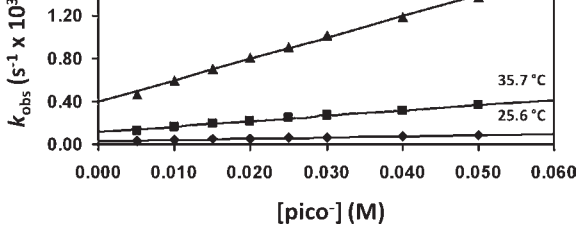

Figure 4. Temperature and [pico$^-$] dependence of the *pseudo*-first-order rate constant (k_{obs}) for the second reaction between $[MnN(H_2O)(CN)_4]^{2-}$ and pico$^-$ anions, $[Mn]_T = 5.26 \times 10^{-4}$ M, μ = 1.0 M (KNO_3), pH = 10.0, λ = 350 nm.

$[MnN(H_2O)(CN)_4]^-$ was therefore obtained from a least-squares fit of this data to eq 3 and is reported in Table 5.[6]

The substitution reactions could not be studied at pH values higher than 12.5 due to a rapid decomposition of the complexes at very high concentrations of OH^-. It is however interesting to note that the observed rate constant increases at higher pH values, similar to that observed for the reaction of $[MoO(H_2O)(CN)_4]^{2-}$ with 1,10-phenanthroline.[45] By using eq 2, a value of 0.0028(11) is obtained for k_3', which is ca. 3 times larger than the k_1' value. This is interpreted as evidence for a potential interchange activation for the cyanido substitution at the hydroxo species, since the Mn−OH bond is much stronger than the Mn−OH_2 bond. In an I_d or even I_a mechanism, the increase in the Mn−OH bond strength implies an increase in electron density at the Mn(V) center, in agreement with an increased dissociation rate for the coordinated cyanido ligand, but also favoring a transition state wherein the association of the picolinate is more prominent prior to the departure of the CN^- ligand. This however necessitates comparable pre-equilibrium contributions, K_3 vs K_1, and is difficult to explain when the system does not allow more detailed study at these higher basic conditions.

It is expected that the slower second ring-closing reaction (Scheme 1) would be independent of both the pH of the solution and the concentration of the entering bidentate ligand. However, this is not the case, since the pH (Figure 5) and ligand concentration (Figure 4 and Supporting Information) both clearly have a significant effect

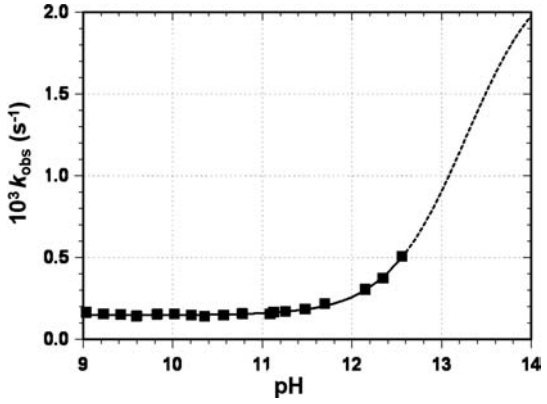

Figure 5. pH dependence of the pseudo-first-order rate constant for the slow reaction between $[MnN(H_2O)(CN)_4]^{2-}$ and 2,3-dipico^{2-} anions at 25.4 °C, $[M]_T = 5.26 \times 10^{-4}$ M, [2,3-dipico$^-$] = 0.080 M, μ = 1.0 M (KNO_3), λ = 365 nm.

on the rate thereof. It is again noted, as mentioned earlier, that the rate of the first reaction could not be determined during the course of this study due to the extremely fast reaction rates and the small accompanying absorbance changes. The observed rate for the ring-closure therefore represents a combined constant as given by eq 2.

It is of interest to note that the rates of substitution observed for all four of the pyridine-carboxylate-type ligands in this study are very similar, which is interpreted as evidence supporting a dissociative activation, see also the further discussion below. The ca. 4 times lower thermodynamic stability of the $[MnN(\eta$-2,3-dipico)$(CN)_4]^{3-}$ complex, as manifested in the stability constants, compared to that of the other three complexes is hard to explain. However, it naturally is assumed to be linked to the COO^- group at the 3 position, exhibiting the most prominent influence, which might be steric or/and electronic, on the K_1 stability constant, more so than the COO^- groups at the 4 and 5 positions of the 2,4- and 2,5-dipico ligands, respectively. This lower stability of the intermediate also indicates the higher energy requirement for the reaction to proceed, as manifested in the higher enthalpy of activation as reported in Table 4.

Table 6 contains a summary of literature data obtained from substitution kinetic studies with bidentate ligands in related d^2 metal centers. Results from the kinetic studies of the substitution reactions between the $[MoO(H_2O)(CN)_4]^{2-}$ complex and the bidentate ligands 1,10-phenanthroline and 2,2′-bipyridine suggested that the *aqua* substitution is the rate-determining step, which is followed by a fast ring-closure as the second step (see Table 6).[45,47] Results from the reported kinetic study of the reaction of the $[WO(H_2O)(CN)_4]^{2-}$ with pyridine-2-carboxylate have however shown that the equilibrium constant (K_1, see reaction C, Scheme 1) for the first reaction is relatively small and in the W(IV) system close to unity.[10]

This may also explain why only one reaction was observed for the two-step reaction between the $[MnN(H_2O)(CN)_4]^{2-}$ complex and the pyridine-2-carboxylate type ligands. Furthermore, since the anation reactions of the $[MnN(H_2O)(CN)_4]^{2-}$ complex are extremely fast,[14] the first reaction would be difficult to observe under the current reaction conditions since the lifetime of $[MnN(\eta^1$-pico$)(CN)_4]^{3-}$ is expected to be too short.

Table 6. Kinetic Data for the Reaction of $[MX(H_2O)(CN)4]^{n-}$ Complexes with Different Bidentate Ligands (LL′) at 25 °C

M	X	LL	pK_{a1}	k_1 (M^{-1} s^{-1})	K'^a (M^{-1})
Mo[b]	O	phen	10.24(7)	0.27(2)	560(30)
	O	bipy		0.26(1)	1.1(1)
W[c]	O	pico$^-$	7.4(2)	$1.80(8) \times 10^{-3}$	13(2)
Re[d]	N	pico$^-$	11.43(2)	$4.20(4) \times 10^{-4}$	3[e]
Mn[f]	N	pico$^-$	13.5(6)[g]	$1.15(4) \times 10^{-3}$	33(4)
	N	2,3-dipico^{2-}		$1.11(1) \times 10^{-3}$	6.4(6)
	N	2,4-dipico^{2-}		$8.5(5) \times 10^{-4}$	30(4)
	N	2,5-dipico^{2-}		$1.08(4) \times 10^{-3}$	43(4)

[a] K' = overall equilibrium constant. [b] Ref 41. [c] Ref 10. [d] Ref 43, calculated at 25 °C. [e] Ref 43, recalculated for overall process at 80 °C. [f] This study. [g] Average from Table 4

The data obtained from eq 2 indicate that these forward rate constants ($k'_1 = k_2K_1$) for the reaction between $[MnN(H_2O)(CN)_4]^{2-}$ and the bidentate pyridine-2-carboxylate ligand compare well with the forward rate constant for the reaction between $[WO(H_2O)(CN)_4]^{2-}$ and pyridine-2-carboxylate ions ($1.80(8) \times 10^{-3}$ s^{-1}). The conclusion therefore is that the equilibrium constants (K_1) of the first reaction for the Mn(V) system are also assumed to be near to unity, similar to that found for the W(IV) system. This is also in agreement with similar results which were obtained for the kinetic study of the reaction of the $[ReN(H_2O)(CN)_4]^{2-}$ with pyridine-2-carboxylate ions, albeit 4 times slower,[43] see Table 6.

In the study of the mentioned Re(V) system, the pK_{a1} value of 11.43(2) for $[ReN(H_2O)(CN)_4]^{2-}$ has been reported. The current study enabled the approximate determination of the pK_{a1} value (= 13.5) for the $[MnN(H_2O)(CN)_4]^{2-}$ for the first time. As a consequence, it may therefore be assumed that the pK_{a1} value for the corresponding fourth row complex $[TcN(H_2O)(CN)_4]^{2-}$ should be ca. 12, in accordance with the basicity of the isostructural $[MO(H_2O)(CN)_4]^{2-}$ complexes [M = Mo(IV), W(IV)].[2]

Activation Parameters. The activation parameters of the overall reaction between the $[MnN(H_2O)(CN)_4]^{2-}$ complex and the different pyridine-2(*x*-di)carboxylate (di)anions were determined by least-squares fits of the temperature-dependent data of the *second*-order rate constant (k'_1) to the Eyring equation and are illustrated in Figure 6 and reported in Table 5.[10]

The second, ring-closing step, involving cyanido substitution, observed $\Delta S_{k1'}^{\ddagger}$ values for the entering bidentate nucleophiles: pyridine-2-carboxylate, 48 ± 3; pyridine-2,3-dicarboxylate, 20 ± 4; pyridine-2,4-dicarboxylate, 115 ± 14; and pyridine-2,5-dicarboxylate, 60 ± 2 J K^{-1} mol^{-1}, respectively, which supports a dissociative activation for this process. Also listed in Table 4 are the activation parameters obtained from a global fit wherein all the k_{obs} values vs [L] vs temperature are fitted into the Eyring equation. This results in probably more representative values for the activation parameters but does not affect the overall signs of the activation entropy and therefore do not affect the overall conclusions.

It is concluded that the slow ring-closing reactions reported here proceed via a dissociative activation, based on the following arguments:

(i) The forward rate constants (k'_1) for the reaction of $[MnN(H_2O)(CN)_4]^{2-}$ with pyridine-2-carboxylate

(47) Samotus, A; Kanas, A; Glug, W.; Szklarzewicz, J. *Trans. Met. Chem.* **1991**, *16*, 614.

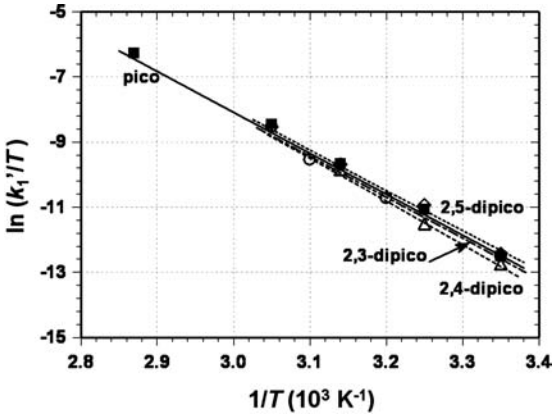

Figure 6. Eyring plot for the reaction between $[MnN(H_2O)(CN)_4]^{2-}$ and the entering ligands pico, 2,3-dipico, 2,4-dipico, and 2,5-dipico.

and the range of 2(*x*-di)carboxylate ligands are remarkably similar (see Figure 6), in spite of a more than a pH unit change in Bronstead basicity (one order-of-magnitude in real terms) of the ligands.

(ii) The rates of the reactions are also virtually independent of the charge of the entering ligand, since the pyridine-2-carboxylato ligand has a 1- charge, while the 2(*x*-di)carboxylate ligands all exhibit −2 charges (all ligands deprotonated at pH = 10 since pK_a values are less than 6[25,26]).

(iii) The activation entropies for the ring-closing reactions studied here are all positive.

The above observations are in agreement with a dissociative activation for the bidentate substitution reactions described here. In such a scenario, the effect of the entering nucleophile will have a relatively small influence on the k'_1 values. Moreover, it has to be noted that the $[MnN(H_2O)(CN)4]^{2-}$ is a classic 18 electron species, which is expected to resist an increase in the coordination number, required for an associative activation. Furthermore, previous studies on corresponding $[MO(H_2O)(CN)_4]^{n-}$ complexes (M = Mo(IV), W(IV), Tc(V), Re(V); X = O^{2-}) indicated that the cyanido exchange proceeds *via* a dissociative process.[48] The rate of the cyanide exchange correlated very well with the rate of the cyanido substitution via bidentate ring-closure,[9,10] indicating that these two processes most probably have CN^- ligand dissociation as the activation step.

(48) Roodt, A.; Leipoldt, J. G.; Helm, L.; Abou-Hamdan, A.; Merbach, A. E. *Inorg. Chem.* **1995**, *34*, 560.

The above is contrary to that reported for the study of $[ReN(H_2O)(CN)_4]^{2-}$ with pyridine-2-carboxylate ions[43] wherein an associative activation was proposed for the ring-closing process.

Conclusions

The dissolution of $[(CH_3)N]_2Na[MnN(CN)_5]\cdot H_2O$ in water results in the dissociation of the labile *trans*-CN^- ligand to form $[MnN(H_2O)(CN)_4]^{2-}$(aq). The *aqua* complex formed reacts rapidly with a number of mono- and bidentate nucleophiles such as *n*-methylpyridines and pyridine-2-carboxylate (pico) and quinoline-2-carboxylate (quino). The molecular structures of $[MnN(\eta^2\text{-pico})(CN)_3]^{2-}$ and $[MnN(\eta^2\text{-quino})(CN)_3]^{2-}$ are reported, indicating that the acid group of the bidentate ligands is positioned *trans* to the nitrido ligand, with the nitrogen in plane with the cyanido ligands.

The kinetics of substitution using pyridine-2-carboxylate and pyridine-2(*x*-di)carboxylate-type ligands showed that the first step in the two-step reaction was too fast to be observed. The second, ring-closing step, involving cyanido substitution, was observed, and kinetic measurements yielded positive values for the activation entropy *and* showed a small dependence on the entering ligand, which supports a dissociative activation for this process. Possible future studies in nonaqueous media utilizing NMR line broadening might shed more light on the first step in this process.

Acknowledgment. Financial assistance from the Research Funds of the Universities of the Free State and Johannesburg, SASOL, THRIP, the NRF, and the UFS Research Cluster Initiative (both the Advanced Biomolecular and the Materials and Nanosciences Clusters) are gratefully acknowledged. Part of this material is based on work supported by the South African National Research Foundation. Opinions, findings, conclusions, or recommendations expressed in this material are those of the authors and do not necessarily reflect the views of the NRF.

Supporting Information Available: Listings of kinetics and equilibrium data (Tables S1−S10, Figures S1−S10). This material is available free of charge via the Internet at http://pubs.acs.org. CCDC data 791911 to 791914 contain the supplementary crystallographic data for this paper. These data can be obtained free of charge via http://ww.ccdc.cam.ac.uk/conts/retrieving.html, or from the Cambridge Crystallographic Data Centre, 12 Union Road, Cambridge CB2 1EZ, U. K.; fax: (+44) 1223−336−033; or e-mail: deposit@ccdc.cam.ac.uk.